A nuclear import pathway exploited by viroid RNAs

Junfei Ma[1], Shachinthaka D. Dissanayaka Mudiyanselage[1], Woong June Park[2], Mo Wang[3,4], Ryuta Takeda[5], Bin Liu[1], Ying Wang[1,*]

[1] Department of Biological Sciences, Mississippi State University, Starkville, MS 39762

[2] Department of Molecular Biology, Dankook University, Chonan-si, Chungnam 31116, Korea

[3] Fujian University Key Laboratory for Plant-Microbe Interaction, Fujian Agriculture and Forestry University, Fuzhou, Fujian 350002, China

[4] Key Laboratory of Ministry of Education for Genetics, Breeding and Multiple Utilization of Crops, College of Agriculture, Fujian Agriculture and Forestry University, Fuzhou, Fujian 350002, China

[5] Leave a Nest Co., Ltd., 5F Iidabashi-Miyuki Bldg, 1-4 Shimomiyabi-cho Shinjuku-Ku, Tokyo 162-0822, Japan

[*] Address correspondence to wang@biology.msstate.edu

Abstract

While most RNAs traffic to the cytoplasm or stay in the nucleus for function, emerging evidence illustrates numerous functional RNAs trafficking in the reverse direction from the cytoplasm to the nucleus. However, the mechanism underlying the RNA nuclear import process has not been well elucidated. Using nuclear-replicating viroids as a model, we showed that cellular Importin alpha-4 and Virp1 likely work in the same pathway for viroid RNA nuclear import. We also demonstrated that a conserved C-loop in nuclear-replicating viroids directly interacts with Virp1 in regulating nuclear import. Further, C-loop exists in a viral satellite RNA that relies on Virp1 for nuclear import. These results have significant implications for understanding the infection process of viroids, a peculiar group of plant pathogens. In addition, our data outline a cellular pathway for the nuclear import of subviral RNAs and uncover a 3-dimensional RNA motif-based regulation over RNA nuclear import.

Introduction

Since most cellular RNAs are produced in the nucleus through transcription in eukaryotic cells, the prevailing view is that those cellular RNAs either stay in the nucleus or move to the cytoplasm via one-way transportation for function. However, emerging evidence showed that cellular RNAs (i.e., small RNAs, tRNAs, and rRNAs), as well as viral RNAs, can traffic in a reverse direction from the cytoplasm to the nucleus. For instance, plant 24-nt hc-siRNAs are exported to the cytoplasm for AGO4 loading before being redirected into the nucleus of the same cell or even neighboring cells for RNA-directed DNA methylation (Long *et al*, 2021; Ye *et al*, 2012). In Xenopus oocytes, 5S rRNA relies on ribosomal protein L5 for nuclear import (Rudt & Pieler, 1996). In another example, satellite RNA of Q-strain cucumber mosaic virus (Q-satRNA) relies on a bromodomain-containing host protein (Virp1) for entering the nucleus (Chaturvedi *et al*, 2014). By and large, in contrast to the well-studied RNA nuclear export process, the RNA nuclear import machinery and mechanism remain obscure.

To cross the double-membrane nuclear envelope, biomolecules need to traffic through the highly organized nuclear pore complexes (NPCs) in eukaryotic cells (Merkle, 2011). NPCs are conserved in eukaryotic organisms with some variations (Meier & Brkljacic, 2009; Xu & Meier, 2008). Except for some free-diffusing small molecules below 40 to 60 kD, most biomolecules rely on nuclear transport receptors (NTRs) to traffic through NPCs (Frey & Gorlich, 2009; Frey *et al*, 2006; Merkle, 2011; Stewart *et al*, 2007). Importin alpha subunits (IMPas) constitute a group of adapter proteins linking specific cargos to NTRs for crossing NPCs (Merkle, 2011). In Arabidopsis thaliana, nine IMPas play distinct yet partially redundant roles (Chen *et al*, 2020; Merkle, 2011). Whether any IMPa is involved in RNA nuclear import remains to be elucidated.

Viroids are single-stranded circular noncoding RNAs that infect plants (Wang, 2021). Due to their noncoding nature, viroids must utilize RNA structures to exploit cellular factors in order to accomplish the infection cycle. Viroid structures have been well annotated via various chemical mapping assays (Gast *et al*, 1996; Giguere *et al*, 2014; Giguere & Perreault, 2017; Xu *et al*, 2012). Recent genome-wide analysis on potato spindle tuber viroid (PSTVd) RNA motifs has identified 11 out of 27 loop motifs responsible for systemic infectivity (Zhong *et al*, 2008). Some of those loop motifs have

been determined as 3D motifs that regulate trafficking across certain cellular boundaries (Takeda *et al*, 2011; Takeda *et al*, 2018; Wu *et al*, 2019; Zhong *et al*, 2007). Viroids of the family *Pospiviroidae* all replicate in the nucleus, and their nuclear import process is highly regulated (Seo *et al*, 2020; Woo *et al*, 1999). Hence, their noncoding RNA genomes must include the necessary information (e.g., an RNA 3D motif) for nuclear import. One viroid binding protein, Virp1, has been implied to accelerate the import of citrus exocortis viroid (CEVd) to nuclei of onion cell strips (Seo *et al*, 2021). Nevertheless, whether and how Virp1 regulates viroid nuclear import await to be clarified.

To gain a better understanding of RNA nuclear import, we test the viroid interaction with all nine IMPas cloned from *Arabidopsis* via RNA-immunoprecipitation and identified IMPa-4 as the specific factor interacting with our model viroid, potato spindle tuber viroid (PSTVd). Down-regulation of IMPa-4 orthologs in tomato led to a drastic reduction of PSTVd infection. We also showed that IMPa-4 interacts with Virp1 in vivo via co-immunoprecipitation. Moreover, we found that Virp1 recognizes a specific RNA 3-dimensional motif, C-loop, in PSTVd, hop stunt viroid (HSVd), and nearly all the nuclear-replicating viroids. Mutational analyses showed that viroid C-loop is critical for infectivity and nuclear import. Notably, C-loop can also be found in the Q-satRNA that relies on Virp1 for nuclear import as well. This work significantly advances our understanding of host-viroid interactions. In addition, our data unravel a novel RNA nuclear import pathway for subviral agents and the molecular basis of a nuclear import signal in RNAs, which have profound implications in understanding the intracellular trafficking of viral RNAs, and potentially cellular RNAs as well.

Results

IMPa-4 is responsible for PSTVd nuclear import

To uncover the specific IMPa protein(s) for PSTVd nuclear import, we employed the RNA-immunoprecipitation assay to determine the PSTVd-binding ability of nine IMPa proteins cloned from *A. thaliana*. As shown in Fig 1A, only IMPa-4 specifically and consistently interacted with PSTVd, as revealed by the presence of PSTVd in the immunoprecipitated fractions via RT-PCR. We chose Histone H2A mRNA (Niben101Scf01866g00004.1) as a negative control for RT-PCR because its homolog in

tomato did not change expression level in PSTVd- or virus-induced gene silencing vector (tobacco rattle virus; TRV)-infected plants in our previous studies (Zheng *et al*, 2017a; Zheng *et al*, 2017c). As shown in Fig 1A, IMPa-4 did not bind with the Histone H2A mRNA, further supporting the specificity in IMPa-4/PSTVd binding. Homology-based analysis showed that IMPa-4 is also present in tomato (Table S1), a host of PSTVd. None of the tomato IMPas have any significant change in expression in PSTVd-infected leaves based on our previously published RNA-Seq data (Table S1), showing that IMPas expression in host plants is not affected by PSTVd infection.

To corroborate the role of IMPa-4 in PSTVd infection, we employed the virus-induced gene silencing assay to specifically down-regulate the IMPa-4 homolog in tomato. The TRV-GFPsil served as a control that did not affect PSTVd infectivity therein (Fig 1B). We cloned an IMPa-4-specific fragment based on the BLAST result and constructed TRV-IMPa-4sil. As expected, the TRV-IMPa-4sil construct strongly suppressed PSTVd accumulation in systemic leaves (Fig 1B). In addition, IMPa-4 expression was suppressed in TRV-IMPa-4sil- but not TRV-GFPsil-treated leaves (Fig 1B). These data confirmed that IMPa-4 is likely a conserved factor facilitating viroid nuclear imports in plants.

IMPa-4 interacts with Virp1

Virp1 was discovered through screening a cDNA library from PSTVd-infected tomato for RNA ligand binding (Martinez de Alba *et al*, 2003) and shown to affect viroid trafficking (Maniataki *et al*, 2003) and replication (Kalantidis *et al*, 2007). Down-regulation of Virp1 is known to attenuate viroid replication in cells (Kalantidis *et al.*, 2007). Recent progress showed that Virp1 is responsible for the nuclear import of Q-satRNA (Chaturvedi *et al.*, 2014) and potentially CEVd (Seo *et al.*, 2021) as well. If Virp1 is critical for viroid nuclear import, it likely functions in the same pathway as IMPa-4. To test this possibility, we employed the co-immunoprecipitation assay to test the interaction between these two proteins. We co-expressed a FLAG-tagged Virp1 construct with TAP-tagged IMPa-4 or IMPa1. As shown in Fig 1C, Virp1 only interacted with IMPa-4 but not IMPa1. Therefore, Virp1 and IMPa-4 likely form a complex and function in the same pathway.

A 3-dimensional RNA motif mediates Virp1 binding with PSTVd

Previous analysis suggested that Virp1 binds to two possible RY motifs in PSTVd (Gozmanova *et al*, 2003), but the structural basis of the RY motif remains elusive. Furthermore, despite that a similar RY motif has been found in another nuclear-replicating viroid HSVd, the overall structures of the RY motif-containing regions between PSTVd and HSVd displayed significant differences (Gozmanova *et al.*, 2003). A close look at the region containing RY motifs in PSTVd showed that there is a C-loop (Fig 2A). C-loop is an asymmetric internal loop, which has the following characteristic features: 1) the first base in the longer strand is often a C; 2) the longer strand has two bases forming non-Watson-Crick (WC) base pairs with bases in the other strand; 3) bases from two strands form two triads; 4) this motif often resides in hairpin stem-loop structure (Drsata *et al*, 2017; Lescoute *et al*, 2005). Interestingly, our preliminary analysis showed that replacing the C-loop with WC base pairs abolished PSTVd nuclear localization signal in *in situ* hybridization analysis (data not shown).

We sought to determine whether this C-loop is the bona fide recognition site of Virp1. Within the PSTVd C-loop (Fig 2A), the cis-WC-Sugar edge interaction between C189 and A173 as well as the trans-WC-Sugar edge interaction between C188 and U186 are flexible for any nucleotide substitution in theory according to the RNA Basepair Catalog (Stombaugh *et al*, 2009), so mutations in these two base pairs may not lead to any conclusive result. Instead, we designed substitutions to replace U187 that may or may not maintain similar trans-WC-Hoogsteen interaction with A171. Alternatively, we replaced the cis-WC-WC basepair U190-A171 with G190-C171. Under this condition, U187 can only be substituted by C187 to maintain the trans-WC-Hoogsteen interaction with the C171 according to the RNA Basepair Catalog. Using these mutational variants, we performed an electrophoretic mobility shift assay (EMSA) using purified Virp1. Interestingly, Virp1 only displayed a strong binding to WT PSTVd in EMSA (Fig 2B and C). Among all the tested variants, all structure-maintaining variants have relatively stronger binding to Virp1 as compared with structure-disruptive variants (Fig 2C).

C-loop is critical for infectivity

As shown in Fig 2D, all PSTVd C-loop disruptive variants and one structure-maintaining mutant (A171C/U187C/U190G) failed to systemically infect *N. benthamiana*.

All these infection defective mutants have a weaker binding to Virp1. Two structure-maintaining mutants, U187A and U187C, showed systemic infection. A careful analysis of the RNA progeny in the systemic leaves revealed that none of the progeny maintained the original sequences as inoculum (Table S2). Nevertheless, nuclear localization is the prerequisite to initiating replication before mutations occur. Therefore, our data still support that the PSTVd structure-maintaining mutants U187A and U187C probably possess the ability to enter the nucleus.

PSTVd C-loop disruptive mutants cannot enter the nucleus

We then analyzed the accumulation patterns of those mutants in local leaves via Whole-Mount *in situ* hybridization because it has been well established that viroid-specific riboprobe can highlight infected nuclei thanks to the high concentration of viroid RNAs (Qi *et al*, 2004; Takeda *et al.*, 2011; Zhong *et al.*, 2007; Zhu *et al*, 2002). As shown in Fig 3, we could not detect PSTVd nuclear accumulation signal in local leaves inoculated with C-loop structure-disruptive variants (i.e., U187G, A171C/U190G, A171C/U187A/U190G, A171C/U187G/U190G). We did not include structure-maintaining mutants (U187A and U187G) because we cannot distinguish the original inoculum and replication products with mutations in our Whole-Mount *in situ* hybridization assay. In contrast, WT PSTVd formed strong signals in the nucleus (Fig 3). In addition, the replication-defective A261C mutant of PSTVd, which still has nuclear import ability (Zhong *et al*, 2006), showed detectable nuclear accumulation as well (Fig 3). The nuclear accumulation signal of A261C in in situ hybridization demonstrated that this assay is sensitive enough to capture imported inoculum without replication. The lack of signal in in situ hybridization is unlikely caused by RNA stability of C-loop variants, as we often observed C-loop variant inoculums in the local leaves 10 days post-infection. To further test RNA stability, we used Argoinfiltration to deliver the cDNAs of C-loop variants into plants. We detected their accumulations comparable to WT transcripts and stronger than the A261C transcripts (Fig S1). Altogether, the in situ hybridization results supported that the C-loop structure-disruptive variants lost their nuclear import ability.

C-loop widely exists in nuclear-replicating viroids

Notably, C-loop can be found in 27 out of 28 formal members and three candidate members of the family *Pospiviroidae* (Fig S2). Based on sequence variations and genomic coordination, we can categorize those viroids into two groups (Fig S2). Interestingly, there are 11 viroids, including PSTVd, containing exactly the same C-loop with identical genomic localization. The remaining 19 viroids in Fig S2 have C-loop structures with diverse sequence variations and genomic localization patterns, which still fit the C-loop model. This observation demonstrates that C-loop is likely a common motif exploited by viroids for nuclear import.

Notably, we also found a variant version of C-loop in HSVd (Fig 4A), a PSTVd relative that has a slightly weaker binding to Virp1 (Maniataki *et al.*, 2003). To test this C-loop variant, we replaced the cis-WC-WC basepair C128-G171 with G-C, A-U, and U-A combinations (Fig 4A). Only the A128-U171 pair is predicted to disrupt the trans-WC-Hoogsteen basepair within the C-loop. Again, all HSVd C-loop variants, one structure-disruptive variant and two structure-maintaining variants, exhibited much-reduced binding to Virp1 (Fig 4B and C). Relatively, both structure-maintaining variants exhibited a slightly stronger binding to Virp1 as compared with the structure-disruptive variant. Since we observed reduced binding in all the mutational designs, we decided to include one more mutant (G157C) as a control, which affects an adjacent loop to the C-loop in HSVd. This mutant now binds to Virp1 comparably to the binding between ViRP1 and WT HSVd (Fig 4B and C).

When we used HSVd C-loop variants and the G157C mutant to infect *N. benthamiana* plants, only G157C can accomplish successful infection (Fig 4D). Sequencing of the progeny confirmed that the G157C mutation was retained in the progeny in systemic leaves (Table S2). Altogether, our observation supports that C-loop is critical for viroid infectivity and Virp1 specifically recognizes viroid C-loop. Since our structure-maintaining mutants showed weak binding to Virp1, it may prefer certain nucleotides in the composition of the C-loop.

Discussion

Proper subcellular localization dictates the function of biomolecules, including various cellular and infectious RNAs. While a majority of cellular RNAs are made in the nucleus

and then either stay in the nucleus or are transported to the cytoplasm for function, numerous RNAs traffic in a reverse direction from the cytoplasm to the nucleus participating in diverse biological processes (Chaturvedi *et al.*, 2014; Chou *et al*, 1998; Gao *et al*, 2012; Kramer & Hopper, 2013; Long *et al.*, 2021; Rudt & Pieler, 1996; Ye *et al.*, 2012). However, the mechanism underlying RNA nuclear import is poorly understood. Here, we present evidence uncovering an IMPa-4-Virp1 pathway (Fig 5) in transporting viroid RNAs from the cytoplasm to the nucleus in plants. Notably, we identified a genetic element, an RNA C-loop, as a critical signal for viral RNA nuclear import. Previous studies suggest that Virp1 recognizes RY motifs in viroids (R: A or G; Y: C or U) (Gozmanova *et al.*, 2003; Maniataki *et al.*, 2003). RY motif and C-loop partially overlap in some viroids, like PSTVd. The drastic changes in binding and infectivity of point mutations that disrupt PSTVd C-loop support the strong role of C-loop for Virp1 recognition. More importantly, HSVd C-loop disruptive mutants that are not overlapping with RY motifs have a much stronger effect on infectivity and Virp1-binding as compared with G157C mutant that overlaps with the RY-motif. Altogether, our data strongly support C-loop as a bona fide signal for selective nuclear import of RNA.

C-loop has been found in many rRNAs (Drsata *et al.*, 2017; Lescoute *et al.*, 2005), a bacterial mRNA (Torres-Larios *et al*, 2002), and some conserved mammalian noncoding RNAs (Iacoangeli & Tiedge, 2013). In general, C-loop increases the local helical twist of RNA helices (Afonin & Leontis, 2006). C-loop in the mRNA and those mammalian noncoding RNAs are involved in translational regulation (Iacoangeli & Tiedge, 2013; Torres-Larios *et al.*, 2002). Our data expand the function of the C-loop and uncover Virp1 as a new protein partner for this RNA motif.

Virp1 was first identified as a PSTVd interacting protein through screening cDNA library from PSTVd-infected tomato for RNA ligand binding (Martinez de Alba *et al.*, 2003). Early work suggests that Virp1 is important for PSTVd systemic trafficking because the binding-deficient PSTVd mutants failed to achieve systemic trafficking (Maniataki *et al.*, 2003). Later on, protoplast assay using Virp1 down-regulated cells suggested that Virp1 has a role in PSTVd replication (Kalantidis *et al.*, 2007). Very recently, Virp1 has been implied to regulate CEVd nuclear import in an in situ assay based on onion cells (Wu *et al.*, 2019). Our data provide compelling evidence supporting a critical role of Virp1 in viroid

nuclear import, facilitated by IMPa-4. Notably, both IMPa-4 and Virp1 have been implicated in T-DNA nuclear import (Bhattacharjee *et al*, 2008; Crane & Gelvin, 2007). It will be interesting to further investigate whether IMPa-4 and Virp1 also participate in viral DNA and/or cellular RNA nuclear import in the future.

Currently, there are 28 formal members of the family *Pospiviroidae* (Di Serio *et al*, 2021), and 27 of them (except citrus dwarfing viroid) possess a C-loop. Eleven viroids, including eight out of nine members in the genus *Pospiviroid* where PSTVd belongs, possess an identical C-loop in their genomes. A close look at the rest of the viroids of the family *Pospiviroidae* suggests the existence of C-loop therein with some variations in sequences and genome localization in all but citrus dwarfing viroid (Fig. S2). Notably, these viroid structures are supported by Selective 2′ Hydroxyl Acylation analyzed by Primer Extension (SHAPE) analysis (Giguere *et al.*, 2014; Giguere & Perreault, 2017; Xu *et al.*, 2012), except for citrus bark cracking viroid and citrus viroid-VI whose structures were predicted using mFOLD (Zuker, 2003). Therefore, a conserved nuclear import signal likely exists in nearly all nuclear-replicating viroids. Interestingly, C-loop variants can also be found in mexican papita viroid, citrus viroid-IV, and grapevine latent viroid, which are candidate members of *Pospiviroidae*. Future functional investigation on those C-loop variants can provide insights into the precise structural basis and critical nucleotide preferences in mediating RNA nuclear import. It is also interesting to analyze citrus dwarfing viroid to test 1) whether it possesses an alternative binding site for Virp1 and/or 2) there is an alternative nuclear import route.

Interestingly, Q-satRNA appears to have a C-loop in its RNA sequence as well. EMSA testing using a C-Loop disruptive Q-satRNA showed significantly reduced binding to Virp1 as compared with that of WT Q-satRNA, further supporting the critical role of C-loop in binding with Virp1 (Fig. S3). Therefore, C-loop-based RNA nuclear import is possibly exploited by infectious RNAs in common. Whether any cellular RNA follows this pathway for nuclear import to exert functions in plants deserves future investigation. Our study paves the way to explore RNA nuclear import machinery and identify genetic information in RNA molecules in determining their subcellular localization. This line of research may lead to future manipulation of RNA subcellular localizations of various RNAs for functional studies and applications.

Materials and Methods

Plant growth

Arabidopsis plants were grown in a growth chamber at 22°C with a 10/14 h light/dark cycle. *N. benthamiana* plants were grown in a growth chamber at 25°C with a 14/10 h light/dark cycle. *N. benthamiana* seedlings at the four-leaf stage were inoculated with water or water containing 150 ng of in vitro transcribed viroid RNAs. The viroid infection was analyzed by RNA gel blots using local leaves 10 days post-inoculation and systemic leaves three weeks post-inoculation as described previously. Agroinfiltration followed an established protocol (Wang *et al*, 2016).

DNA clones

cDNAs of some Arabidopsis Importin alpha subunits in pC-TAPa or Lic6 vectors were purchased from ABRC (Ohio State University, Columbus, OH): IMPa1 (DKLAT3G06720), IMPa2 (DKLAT4G16143), IMPa3 (DKLAT4G02150), IMPa-4 (DKLAT1G09270), IMPa5 (DKLAT5G49310.1) and IMPa6 (DKLAT1G02690). IMPa7 cDNA in pDONR221 vector (DQ446636) was purchased from ABRC and recombinated into pC-TAPa vector (ABRC) via LR clonase (Thermo Fisher Scientific, Waltham, MA). IMPa8 and IMPa9 were amplified using gene-specific primers (Table S3) and cloned into pCR8 (Thermo Fisher Scientific), which were then recombinated into pC-TAPa via LR clonase.

To generate the pTRV2-IMPa-4sil clone, two specific primers (Table S3) for *N. benthamiana* IMPa-4 fragment were used for genomic PCR and followed by digestion with *BamH*I and *Xho*I (New England Biolabs, Ipswich, MA). The pTRV2 vector (ABRC) linearized by *BamH*I and *Xho*I were used for ligation with the digested NbIMPa-4 fragments. Since we cannot reach 100% PSTVd infection in *N. benthamiana*, we then decided to use tomato for the VIGS assay. Based on the high sequence homology of IMPa-4 in tomato and *N. benthamiana*, we used the same pTRV2-IMPa-4sil clone for infiltration. Based on the BLAST search using Sol genomics database (https://solgenomics.net), our cloned fragment specifically targets IMPa-4 homologs in tomato and *N. benthamiana*. pTRV2 variants in agrobacterium GV3101 were mixed with Agrobacterium harboring pTRV1 (ABRC) for VIGS infiltration into one cotyledon of tomato

seedlings, while the other cotyledon was used for inoculation with PSTVd RNA transcripts. Plants were subjected to RNA gel blot to analyze PSTVd and TRV titers, as well as the expression levels of IMPa-4 and Histone H2A (see Table S2 for primer details). The TRV probe was described previously (Zheng *et al.*, 2017a).

Virp1 from Arabidopsis was cloned via RT-PCT using gene-specific primers (Table S3). The cloned Virp1 cDNA was inserted in pCR8 vector and then recombinated into pMDC7 vector (modified to include a N-FLAG tag; inherited from Biao Ding at Ohio State University) for agroinfiltration or pDEST15 vector (Thermo Fisher Scientific) for bacterial expression, via LR clonase. GST construct for bacterial expression was a gift from Svetlana Folimonova at University of Florida.

The cDNAs of WT and mutant Q-satRNAs were commercially synthesized (Genscript, Piscataway, NJ). The cDNAs were amplified (see Table S3 for primers) and ligated into pGEM-T vector (Promega, Madison, WI). To generate RNA substrates for EMSA, *Spe*I (New England Biolabs) linearized plasmids (pGEMT-Q-satRNA^{WT} and pGEMT-Q-satRNA^{mu}) were subject to *in vitro* transcription using T7 MEGAscript kit (Thermo Fisher Scientific).

To generate RNA inocula, pRZ:Int construct (Wang *et al*, 2007) was by *Hind*III (New England Biolabs) followed by *in vitro* transcription using T7 MEGAscript kit. pT3:HSVd^{RZ} (Tu HSVd2-7 in the 83-82 orientation) used pGEM-T vector with the insertion cloned from HSVd-RZ (a gift from Dr. Robert Owens at USDA-ARS) via T3-HSVd-f and RZ-r primers (Table S3). pT3:HSVd^{RZ} was linearized by *Hind*III followed by *in vitro* transcription using T3 MEGAscript kit (Thermo Fisher Scientific). All RNA *in vitro* transcripts were purified using the MEGAclear kit (Thermo Fisher Scientific).

To generate Riboprobes, pInt(-) (Zheng *et al*, 2017b) was linearized by *Spe*I (New England Biolabs) as the template and T7 MAXIscript kit (Thermo Fisher Scientific) was used to generate probe. pHSVd-monomer was based on pGEM-T vector (Promega) via insertion of HSVd cDNA cloned from HSVd-RZ plasmid via HSVd-f and HSVd-r primers (Table S3). The pHSVd-Monomer was linearized by *Nco*I (New England Biolabs) as the template and SP6 MAXIscript kit (Thermo Fisher Scientific) was used to generate probe. To generate Q-satRNA probe, pGEMT-Q-satRNA^{WT} was linearized by *Nco*I (New England Biolabs) and subject to in vitro transcription using SP6 MAXIscript kit.

To generate WT, A261C, and C-loop mutant constructs for agroinfiltration, the corresponding pRZ:Int plasmids harboring the correct PSTVd cDNAs served as templates for PCR (using RZ-f and RZ-r primers; see Table S3 for primer sequences). The PCR products were inserted into pENTR-D-TOPO vector (Thermo Fisher Scientific). The series of pENTR-RZ:Int plasmids were recombinated into CD3-1656 (ABRC) via LR clonase. The CD3-1656-RZ:Int plasmid series were transformed into Agrobacterium strain GV3101 for agroinfiltration.

All the constructs have been verified using Sanger sequencing.

RNA immunoprecipitation

RNA-immunoprecipitation (RIP) was performed according to a previously described protocol (Wang *et al.*, 2016) with minor modifications. Briefly, PSTVd-infected leaves were harvest 3 days post agroinfiltration of Importin alpha cDNAs. The cell lysates were incubated with magnetic mouse IgG beads (Cell Signaling, Danvers, MA) for 2 h at 4°C. The input lysate and purified fractions were subject to immunoblotting and RT-PCR (after RNA purification). The primers for detecting PSTVd and Histone 2A mRNA were listed in Table S3.

Co-Immunoprecipitation

Co-immunoprecipitation was following a recent report (Chen *et al.*, 2020) with minor modifications. FLAG-tagged Virp1 was co-expressed with MYC-tagged IMPa1 or IMPa-4 via agroinfiltration. Three days post infiltration, 4 mM 17-b-estradiol was infiltrated in leaves 6 h before sampling. The cell lysates from leaf samples were incubated with anti-FLAG antibody for 1 h at 4°C. The magnetic protein A/G beads (Thermo Fisher Scientific) were then added to the lysate for another 1 h incubation at 4°C with mild shaking. The beads were washed twice with 1X PBST buffer (137 mM NaCl, 2.7 mM KCl, 10 mM Na_2HPO_4, 1.8 mM KH_2PO_4, 0.1% Triton X-100) and once with distilled water. The bound proteins were eluted using IgG elution buffer (Thermo Fisher Scientific) and then subject to immunoblots.

Protein purification

GST and Recombinant Virp1-GST proteins were expressed in *Escherichia coli* Rosetta strain (EMD Millipore, Burlington, MA). Cells were grown overnight at 37°C in LB media supplied with ampicillin (0.1 mg/ml) and chloramphenicol (0.034 mg/ml). An aliquot of cells with OD600 = 0.1 was inoculated into fresh LB supplied with antibiotics the next day. Once the cell density (OD600) reached 0.5-0.7, 0.4 mM IPTG (final concentration) was added to the culture to induce protein expression. After inducing at 20°C overnight, 100 ml culture was harvested by centrifugation at 8,000 rpm for 8 min. Pellets were re-suspended in 1X PBS buffer (137 mM NaCl, 2.7 mM KCl, 10 mM Na_2HPO_4, and 1.8 mM KH_2PO_4) supplement with 20 mM PMSF and sonicated to lyse the cells. The cell lysate was then centrifuged at 10,800 rpm for 30 min at 4°C. The supernatant was collected and incubated for 1 h with 2 ml of 50% slurry of Glutathione Resin (Genscript) before loading onto an empty EconoPac gravity-flow column (Bio-Rad Laboratories, Hercules, CA). The resin was then washed with 10 mL 1xPBS followed by applying 10 mL elution buffer (50 mM Tris-HCl pH 8.0 and 10 mM reduced glutathione). The elutes were concentrated using an Amicon protein concentrator (MilliporeSigma, Burlington, MA). Proteins were then separated by 8% SDS-PAGE electrophoresis followed by Coomassie blue staining and de-staining to estimate concentration using a BSA standard as reference.

Electrophoresis mobility shifting assays (EMSAs)

The detailed protocol has been reported previously (Gozmanova *et al.*, 2003). Binding assays that contained RNA in the absence or presence of different amounts of GST or Virp1-GST proteins were incubated at 28°C for 30 min. The binding buffer was composed of 10 mM HEPES-NaOH (pH 8.0), 50 mM KCl, 100 mM EDTA, and 5% glycerol. Electrophoresis for the binding assay was performed on ice in 6% polyacrylamide (29:1) gels at 140 V using 0.5X TBE (50 mM Tris, 50 mM boric acid, 1 mM EDTA, pH 8.3) for 1.6 h. The following steps are described below in the RNA gel blots section. The percentage of shifted variant RNAs was normalized to that of WT RNAs to infer a relative binding strength to Virp1, based on at least three replicates.

Tissue processing and in situ hybridization

The tissue fixation and processing were largely described previously (Takeda *et al.*, 2011) with minor modification. Briefly, 8 DPI leaf samples were fixed in FAA solution (50% ethanol/5% formaldehyde/5% acetic acid) for 30 min and then dehydrated by a step-wise gradient of ethanol solutions. The samples were washed by 1XPBS and treated with 10 mg/mL of proteinase K for 20 min at 37°C. Then, the samples were hybridized with Dig-labeled antisense riboprobes (generated as above-mentioned) at 50°C overnight. The samples were washed, incubated with anti-DIG monoclonal antibody (MilliporeSigma) and NBT/BCIP substrate (MilliporeSigma) subsequentially, and mounted with Permount (Thermo Fisher Scientific) for visualization using an Olympus CX23 light microscope. The scale bars were calculated using ImageJ (https://imagej.nih.gov/ij/).

RNA gel blots and immunoblots

After electrophoresis, RNAs were then transferred to Hybond-XL nylon membranes (Amersham Biosciences, Little Chalfont, United Kingdom) via a semi-dry transfer cassette (Bio-Rad Laboratories) and were immobilized by a UV-crosslinker (UVP, Upland, CA). RNAs were then detected by DIG-labeled UTP probes. AP-conjugated anti-DIG monoclonal antibody was used in combination with Immun-Star substrates (Bio-Rad Laboratories). Signals were captured by ChemiDoc (Bio-Rad Laboratories).

After SDS-PAGE electrophoresis, we followed the previously described protocol for immunoblotting (Jiang *et al*, 2019). IMPas were detected by a monoclonal mouse anti-Myc antibody (MilliporeSigma; 1:3,000 dilution). Virp1 was detected by a monoclonal mouse anti-FLAG antibody (Thermo Fisher Scientific; 1:1,000 dilution). HRP-conjugated anti-mouse serum (Bio-Rad Laboratories) was diluted at 1:2000. SuperSignal West Dura (Thermo Fisher Scientific) was used as the substrate. Signals were captured by ChemiDoc (Bio-Rad Laboratories).

Data availability

The published RNA-Seq dataset has been deposited in the NCBI SRA with accession number SRP093503.

Acknowledgements

This work was supported by grants from the US National Science Foundation (MCB-1906060 to YW) and the US National Institute of General Medical Sciences (1R15GM135893 to YW). We are indebted to Robert Owens (USDA-ARS) and Svetlana Folimonova (University of Florida) for their gifts of DNA constructs. We are grateful for the constructive comments from Donna Gordon (Mississippi State University). We thank Laxmi Kharel (Mississippi State University) for technical support. This work is dedicated to the late Professors Biao Ding (Ohio State University) and Neocles B. Leontis (Bowling Green State University), who participated at the inception stage.

Author contributions

RT and YW conceived the study. YW designed the experiments. JM, SDM, and YW performed the experiments. JM and YW analyzed the data. YW wrote the manuscript. MJ, WJP, MW, BL, and YW discussed the results and revised the manuscript.

Conflict of interest

The authors declare that they have no conflict of interest.

Reference

Afonin KA, Leontis NB (2006) Generating new specific RNA interaction interfaces using C-loops. *J Am Chem Soc* 128: 16131-16137

Bhattacharjee S, Lee LY, Oltmanns H, Cao H, Veena, Cuperus J, Gelvin SB (2008) IMPa-4, an Arabidopsis importin alpha isoform, is preferentially involved in agrobacterium-mediated plant transformation. *Plant Cell* 20: 2661-2680

Chaturvedi S, Kalantidis K, Rao AL (2014) A bromodomain-containing host protein mediates the nuclear importation of a satellite RNA of Cucumber mosaic virus. *J Virol* 88: 1890-1896

Chen C, Kim D, Yun HR, Lee YM, Yogendra B, Bo Z, Kim HE, Min JH, Lee YS, Rim YG *et al* (2020) Nuclear import of LIKE HETEROCHROMATIN PROTEIN1 is redundantly mediated by importins alpha-1, alpha-2 and alpha-3. *Plant J* 103: 1205-1214

Chou HC, Hsieh TY, Sheu GT, Lai MM (1998) Hepatitis delta antigen mediates the nuclear import of hepatitis delta virus RNA. *J Virol* 72: 3684-3690

Crane YM, Gelvin SB (2007) RNAi-mediated gene silencing reveals involvement of Arabidopsis chromatin-related genes in Agrobacterium-mediated root transformation. *Proc Natl Acad Sci U S A* 104: 15156-15161

Di Serio F, Owens RA, Li SF, Matousek J, Pallas V, Randles JW, Sano T, Verhoeven JTJ, Vidalakis G, Flores R *et al* (2021) ICTV Virus Taxonomy Profile: Pospiviroidae. *J Gen Virol* 102

Drsata T, Reblova K, Besseova I, Sponer J, Lankas F (2017) rRNA C-Loops: Mechanical Properties of a Recurrent Structural Motif. *J Chem Theory Comput* 13: 3359-3371
Frey S, Gorlich D (2009) FG/FxFG as well as GLFG repeats form a selective permeability barrier with self-healing properties. *Embo J* 28: 2554-2567
Frey S, Richter RP, Gorlich D (2006) FG-rich repeats of nuclear pore proteins form a three-dimensional meshwork with hydrogel-like properties. *Science* 314: 815-817
Gao R, Liu P, Wong SM (2012) Identification of a plant viral RNA genome in the nucleus. *PLoS One* 7: e48736
Gast FU, Kempe D, Spieker RL, Sanger HL (1996) Secondary structure probing of potato spindle tuber viroid (PSTVd) and sequence comparison with other small pathogenic RNA replicons provides evidence for central non-canonical base-pairs, large A-rich loops, and a terminal branch. *J Mol Biol* 262: 652-670
Giguere T, Adkar-Purushothama CR, Perreault JP (2014) Comprehensive secondary structure elucidation of four genera of the family Pospiviroidae. *PLoS One* 9: e98655
Giguere T, Perreault JP (2017) Classification of the Pospiviroidae based on their structural hallmarks. *PLoS One* 12: e0182536
Gozmanova M, Denti MA, Minkov IN, Tsagris M, Tabler M (2003) Characterization of the RNA motif responsible for the specific interaction of potato spindle tuber viroid RNA (PSTVd) and the tomato protein Virp1. *Nucleic Acids Res* 31: 5534-5543
Iacoangeli A, Tiedge H (2013) Translational control at the synapse: role of RNA regulators. *Trends Biochem Sci* 38: 47-55
Jiang J, Ma J, Liu B, Wang Y (2019) Combining a Simple Method for DNA/RNA/Protein Co-Purification and Arabidopsis Protoplast Assay to Facilitate Viroid Research. *Viruses* 11
Kalantidis K, Denti MA, Tzortzakaki S, Marinou E, Tabler M, Tsagris M (2007) Virp1 is a host protein with a major role in Potato spindle tuber viroid infection in Nicotiana plants. *J Virol* 81: 12872-12880
Kramer EB, Hopper AK (2013) Retrograde transfer RNA nuclear import provides a new level of tRNA quality control in Saccharomyces cerevisiae. *Proc Natl Acad Sci U S A* 110: 21042-21047
Lescoute A, Leontis NB, Massire C, Westhof E (2005) Recurrent structural RNA motifs, Isostericity Matrices and sequence alignments. *Nucleic Acids Res* 33: 2395-2409
Long J, Walker J, She W, Aldridge B, Gao H, Deans S, Vickers M, Feng X (2021) Nurse cell--derived small RNAs define paternal epigenetic inheritance in Arabidopsis. *Science* 373
Maniataki E, Martinez de Alba AE, Sagesser R, Tabler M, Tsagris M (2003) Viroid RNA systemic spread may depend on the interaction of a 71-nucleotide bulged hairpin with the host protein VirP1. *RNA* 9: 346-354
Martinez de Alba AE, Sagesser R, Tabler M, Tsagris M (2003) A bromodomain-containing protein from tomato specifically binds potato spindle tuber viroid RNA in vitro and in vivo. *J Virol* 77: 9685-9694
Meier I, Brkljacic J (2009) Adding pieces to the puzzling plant nuclear envelope. *Curr Opin Plant Biol* 12: 752-759
Merkle T (2011) Nucleo-cytoplasmic transport of proteins and RNA in plants. *Plant Cell Rep* 30: 153-176

Qi Y, Pélissier T, Itaya A, Hunt E, Wassenegger M, Ding B (2004) Direct role of a viroid RNA motif in mediating directional RNA trafficking across a specific cellular boundary. *Plant Cell* 16: 1741-1752
Rudt F, Pieler T (1996) Cytoplasmic retention and nuclear import of 5S ribosomal RNA containing RNPs. *Embo J* 15: 1383-1391
Seo H, Kim K, Park WJ (2021) Effect of VIRP1 Protein on Nuclear Import of Citrus Exocortis Viroid (CEVd). *Biomolecules* 11
Seo H, Wang Y, Park WJ (2020) Time-Resolved Observation of the Destination of Microinjected Potato Spindle Tuber Viroid (PSTVd) in the Abaxial Leaf Epidermal Cells of Nicotiana benthamiana. *Microorganisms* 8
Stewart CL, Roux KJ, Burke B (2007) Blurring the boundary: the nuclear envelope extends its reach. *Science* 318: 1408-1412
Stombaugh J, Zirbel CL, Westhof E, Leontis NB (2009) Frequency and isostericity of RNA base pairs. *Nucleic Acids Res* 37: 2294-2312
Takeda R, Petrov AI, Leontis NB, Ding B (2011) A three-dimensional RNA motif in Potato spindle tuber viroid mediates trafficking from palisade mesophyll to spongy mesophyll in Nicotiana benthamiana. *Plant Cell* 23: 258-272
Takeda R, Zirbel CL, Leontis NB, Wang Y, Ding B (2018) Allelic RNA Motifs in Regulating Systemic Trafficking of Potato Spindle Tuber Viroid. *Viruses* 10
Torres-Larios A, Dock-Bregeon AC, Romby P, Rees B, Sankaranarayanan R, Caillet J, Springer M, Ehresmann C, Ehresmann B, Moras D (2002) Structural basis of translational control by Escherichia coli threonyl tRNA synthetase. *Nat Struct Biol* 9: 343-347
Wang Y (2021) Current view and perspectives in viroid replication. *Curr Opin Virol* 47: 32-37
Wang Y, Qu J, Ji S, Wallace AJ, Wu J, Li Y, Gopalan V, Ding B (2016) A Land Plant-Specific Transcription Factor Directly Enhances Transcription of a Pathogenic Noncoding RNA Template by DNA-Dependent RNA Polymerase II. *Plant Cell* 28: 1094-1107
Wang Y, Zhong X, Itaya A, Ding B (2007) Evidence for the Existence of the Loop E Motif of Potato Spindle Tuber Viroid In Vivo ▿ . *Journal of Virology* 81: 2074-2077
Woo Y-M, Itaya A, Owens RA, Tang L, Hammond RW, Chou H-C, Lai MMC, Ding B (1999) Characterization of nuclear import of potato spindle tuber viroid RNA in permeabilized protoplasts. *The Plant Journal* 17: 627-635
Wu J, Leontis NB, Zirbel CL, Bisaro DM, Ding B (2019) A three-dimensional RNA motif mediates directional trafficking of Potato spindle tuber viroid from epidermal to palisade mesophyll cells in Nicotiana benthamiana. *PLoS Pathog* 15: e1008147
Xu W, Bolduc F, Hong N, Perreault JP (2012) The use of a combination of computer-assisted structure prediction and SHAPE probing to elucidate the secondary structures of five viroids. *Mol Plant Pathol* 13: 666-676
Xu XM, Meier I (2008) The nuclear pore comes to the fore. *Trends Plant Sci* 13: 20-27
Ye R, Wang W, Iki T, Liu C, Wu Y, Ishikawa M, Zhou X, Qi Y (2012) Cytoplasmic assembly and selective nuclear import of Arabidopsis Argonaute4/siRNA complexes. *Mol Cell* 46: 859-870
Zheng Y, Ding B, Fei Z, Wang Y (2017a) Comprehensive transcriptome analyses reveal tomato plant responses to tobacco rattle virus-based gene silencing vectors. *Sci Rep* 7: 9771
Zheng Y, Wang Y, Ding B, Fei Z (2017b) Comprehensive Transcriptome Analyses Reveal that Potato Spindle Tuber Viroid Triggers Genome-Wide Changes in Alternative Splicing, Inducible

trans-Acting Activity of Phased Secondary Small Interfering RNAs, and Immune Responses. *J Virol* 91
Zheng Y, Wang Y, Ding B, Fei Z (2017c) Comprehensive transcriptome analyses reveal that potato spindle tuber viroid triggers genome-wide changes in alternative splicing, inducible trans-acting activity of phasiRNAs and immune responses. *J Virol*
Zhong X, Archual AJ, Amin AA, Ding B (2008) A genomic map of viroid RNA motifs critical for replication and systemic trafficking. *Plant Cell* 20: 35-47
Zhong X, Leontis N, Qian S, Itaya A, Qi Y, Boris-Lawrie K, Ding B (2006) Tertiary structural and functional analyses of a viroid RNA motif by isostericity matrix and mutagenesis reveal its essential role in replication. *J Virol* 80: 8566-8581
Zhong X, Tao X, Stombaugh J, Leontis N, Ding B (2007) Tertiary structure and function of an RNA motif required for plant vascular entry to initiate systemic trafficking. *Embo J* 26: 3836-3846
Zhu Y, Qi Y, Xun Y, Owens R, Ding B (2002) Movement of potato spindle tuber viroid reveals regulatory points of phloem-mediated RNA traffic. *Plant Physiol* 130: 138-146
Zuker M (2003) Mfold web server for nucleic acid folding and hybridization prediction. *Nucleic Acids Res* 31: 3406-3415

Figure legends

Figure 1 IMPa-4 and Virp1 in the same pathway for PSTVd infection. A) RNA-immunoprecipitation. TAP-tagged IMPa genes were used to pull down RNAs, which were detected by RT-PCR. Histone H2A serves as a negative control. NC, negative control. IP, immunoprecipitated fraction. B) RNA gel blots showing PSTVd and TRV accumulation in infiltrated leaves. RT-PCR showing the specific downregulation of IMPa-4 by the TRV-IMPa-4Sil construct. C) Co-immunoprecipitation. FLAG-tagged Virp1 serves a bait to pull down IMPa proteins. IP, immunoprecipitated fraction. H2A, histone H2A. NC, negative control.

Figure 2 Characterizing PSTVd C-loop using mutagenesis. A) Rational for C-loop mutant designs. Red crosses indicate that those pairings cannot form in theory. B) EMSA illustrating the interaction between C-loop mutants and Virp1. C) Box plot showing quantification of EMSA results that infer the relative affinities of mutant RNAs to Virp1 as compared to that of WT RNA. D) RNA gel bots detecting the PSTVd systemic infection in *N. benthamiana*. WT PSTVd serves as positive control. Ethidium bromide staining of rRNAs serve as loading control.

Figure 3 C-loop structure-disruptive mutants failed to accumulate in the nucleus. The purple signals in the whole-mount in situ hybridization show the presence of viroid RNAs in the nuclei. There was no signal in non-infected samples or samples infected with C-loop structure-disruptive mutants, in contrast to the samples infected by WT and A261C mutant. Scale bars, 109 μm. Red arrows indicate a few examples of PSTVd-accumulated nuclei.

Figure 4 Characterizing a C-loop variant in HSVd. A) Rational for C-loop mutant designs. B) EMSA illustrating the interaction between C-loop mutants and Virp1. C) Box plot showing quantification of EMSA results that infer the relative affinities of mutant RNAs to Virp1 as compared to that of WT RNA. D) RNA gel bots detecting the HSVd systemic infection in *N. benthamiana*. WT HSVd serves as positive controls. Ethidium bromide staining of rRNAs serves as loading control.

Figure 5 A working model illustrating the IMPa-4/Virp1/C-loop based RNA nuclear import.

Expanded view figure legends

Figure S1 The RNA stability of PSTVd C-loop variants. C-loop mutants, in comparison to wildtype (WT) and A261C mutant, were expressed in *N. benthamiana* via agroinfiltration using CaMV 35S promoter driven RZ:Int-based constructs. Total RNAs from 4 days post infiltrated leaves were run in 2% agarose gel and blotted with PSTVd specific ribo-probes. Ethidium bromide staining of rRNAs serves as loading control. NC, negative control.

Figure S2 C-loop in nuclear-replicating viroids. Illustration of viroid C-loop sequences and relative genomic loci. Viroids whose names are in brown belong to the genus *Pospiviroid*. Viroids whose names in blue were considered but not confirmed as members of the family *Pospiviroidae* in the latest taxonomy.

Figure S3 ViRP1 interaction with Q-satRNA. A) Rational for C-loop mutant designs. B) EMSA illustrating that C-loop disruptive mutant C235G significantly reduced Q-satRNA

binding with Virp1. C) Box plot showing quantification of EMSA results that infer the relative affinity of C235G RNA to Virp1 as compared to that of WT RNA.

Table S1. IMPa homologs in tomato. The normalized reads (FPKM) of tomato IMPas in RNA-Seq dataset are listed. NA, not found.

Table S2. PSTVd and HSVd progeny in systemic leaves.

Table S3. Primer sequences. Nb, Nicotiana benthamiana. Sl, Solanum lycopersicum (tomato).

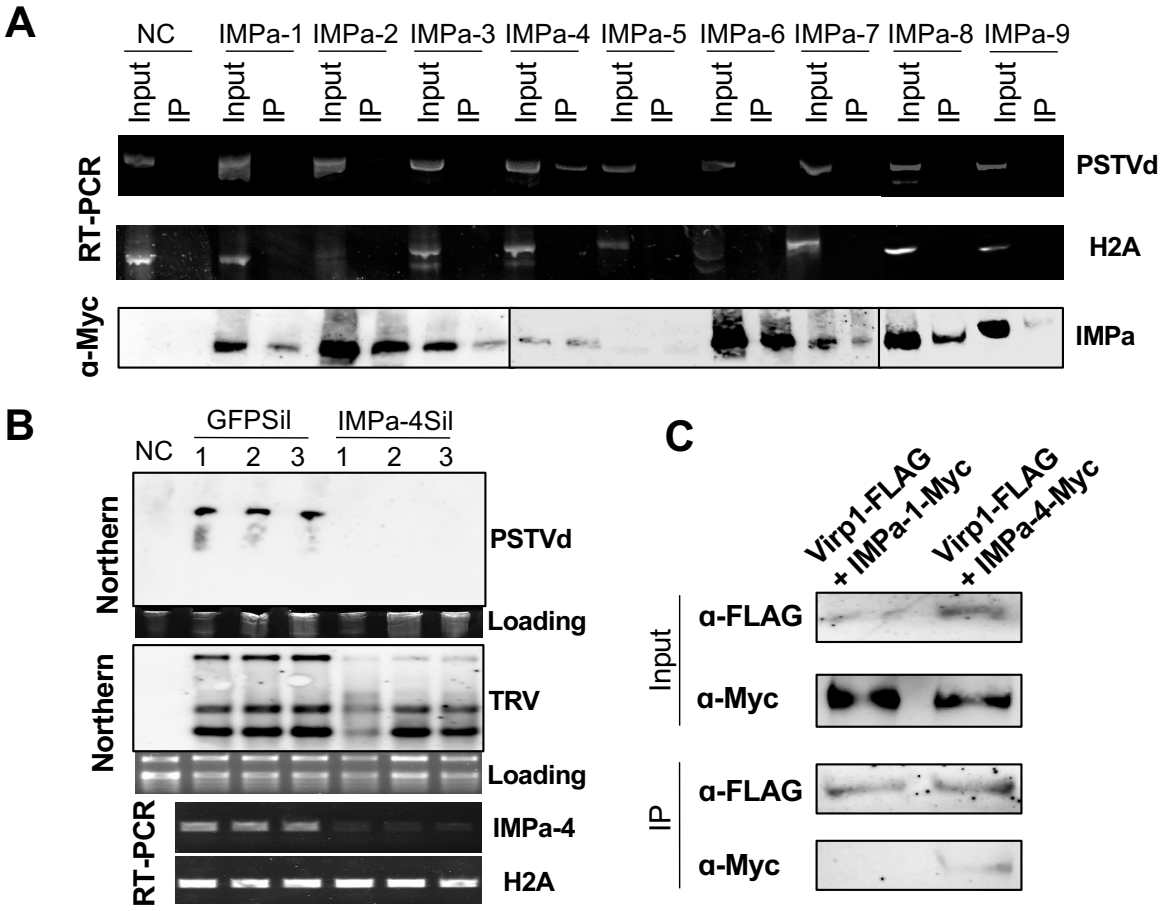
A
NC
IMPa-1
IMPa-2
IMPa-3
IMPa-4
IMPa-5
IMPa-6
IMPa-7
IMPa-8
IMPa-9
Input
IP
RT-PCR
PSTVd
H2A
α-Myc
IMPa
B
GFPSil
IMPa-4Sil
NC
1 2 3 1 2 3
Northern
PSTVd
Loading
Northern
TRV
Loading
RT-PCR
IMPa-4
H2A
C
Virp1-FLAG + IMPa-1-Myc
Virp1-FLAG + IMPa-4-Myc
Input
α-FLAG
α-Myc
IP
α-FLAG
α-Myc

Figure 1

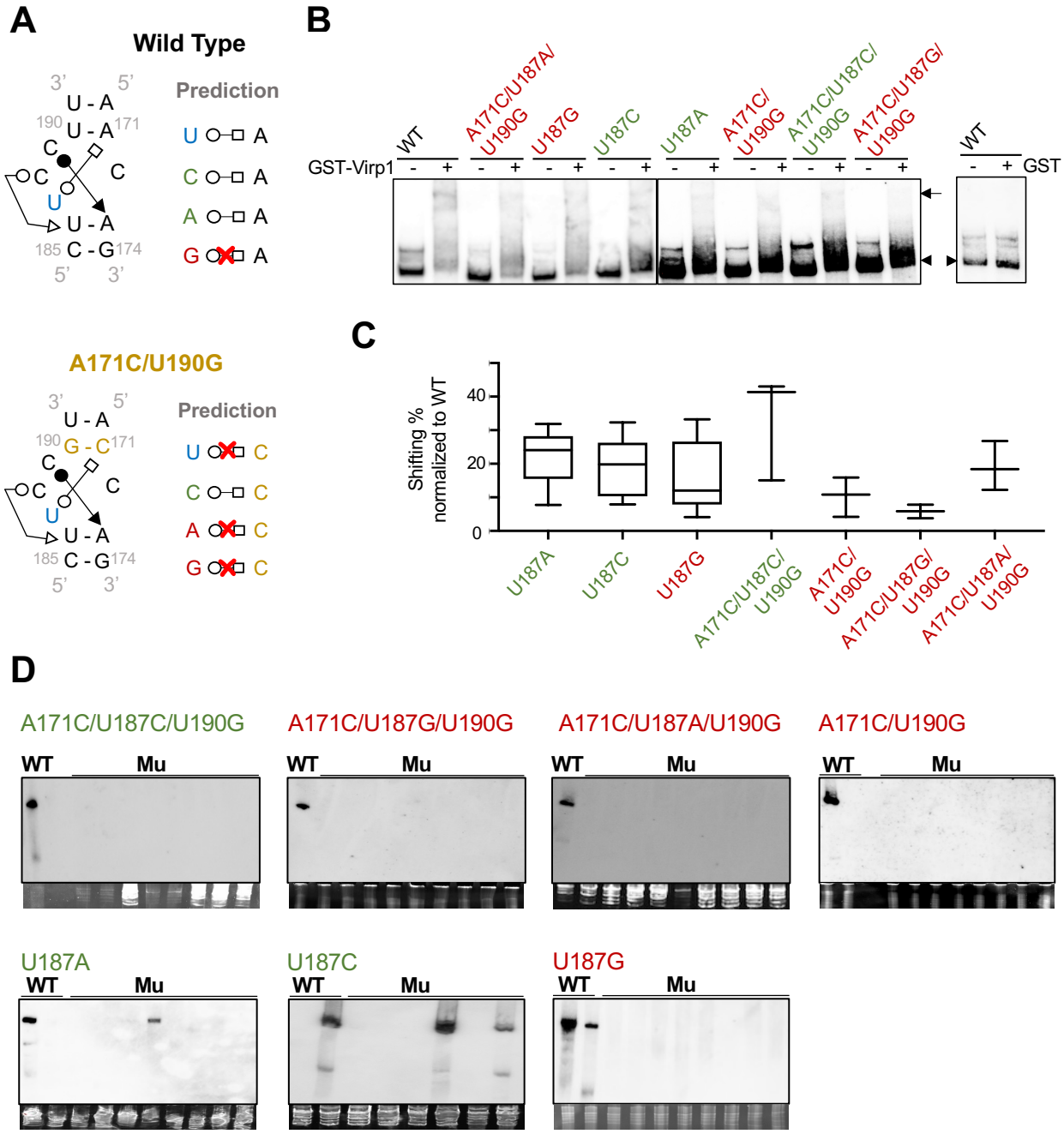
A
Wild Type
Prediction
3' 5'
U - A
190 U - A 171
C
C
C
U
U - A
185 C - G 174
5' 3'
U A
C A
A A
G A
A171C/U190G
Prediction
3' 5'
U - A
190 G - C 171
C
C
C
U
U - A
185 C - G 174
5' 3'
U C
C C
A C
G C
B
GST-Virp1
WT
A171C/U187A/ U190G
U187G
U187C
U187A
A171C/ U190G
A171C/U187C/ U190G
A171C/U187G/ U190G
WT
GST
C
Shifting % normalized to WT
40
20
0
U187A
U187C
U187G
A171C/U187C/ U190G
A171C/ U190G
A171C/U187G/ U190G
A171C/U187A/ U190G
D
A171C/U187C/U190G
A171C/U187G/U190G
A171C/U187A/U190G
A171C/U190G
WT
Mu
U187A
U187C
U187G

Figure 2

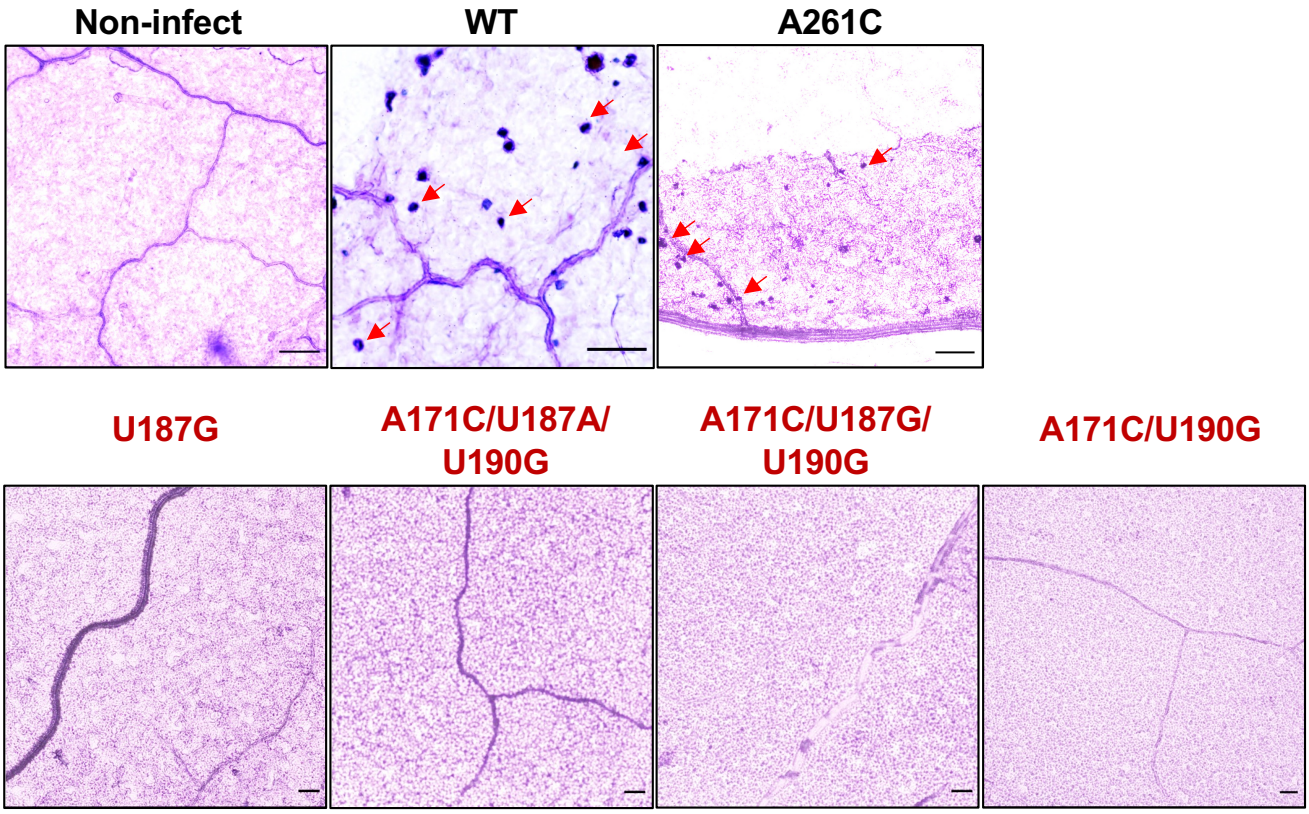
Non-infect
WT
A261C
U187G
A171C/U187A/
U190G
A171C/U187G/
U190G
A171C/U190G

Figure 3

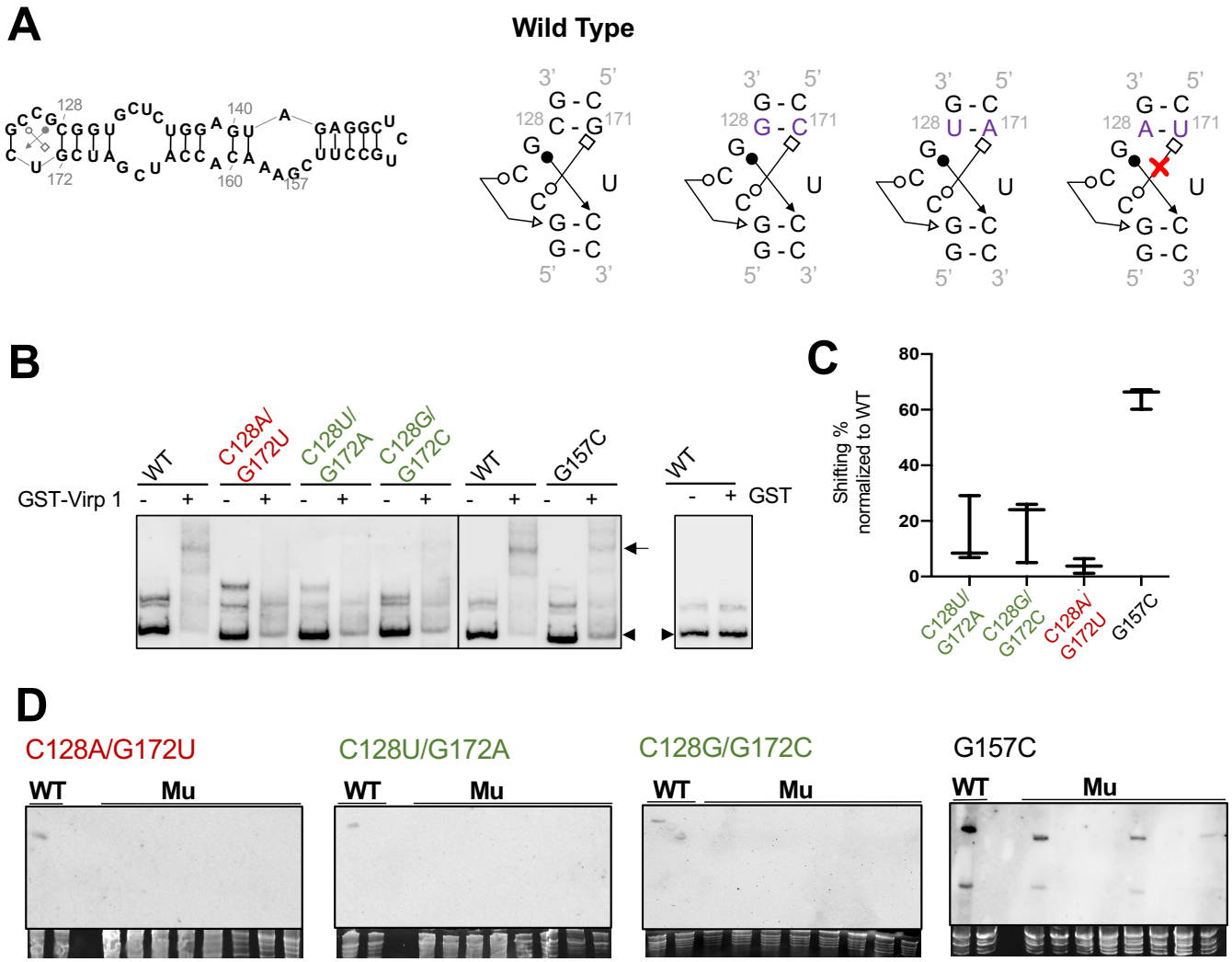
A
Wild Type
B
WT
C128A/ G172U
C128U/ G172A
C128G/ G172C
WT
G157C
WT
GST-Virp 1
GST
C
Shifting % normalized to WT
80
60
40
20
0
C128U/ G172A
C128G/ G172C
C128A/ G172U
G157C
D
C128A/G172U
C128U/G172A
C128G/G172C
G157C
WT
Mu

Figure 4

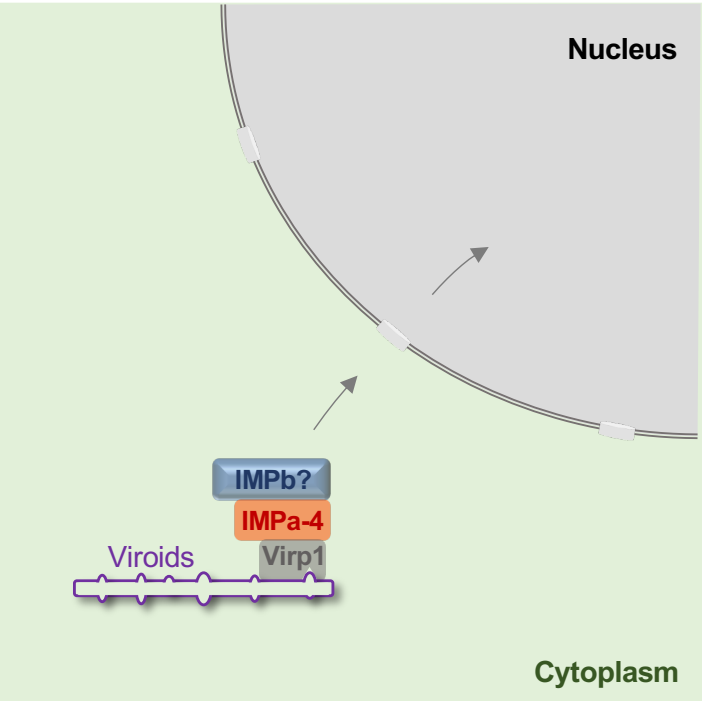

Figure 5

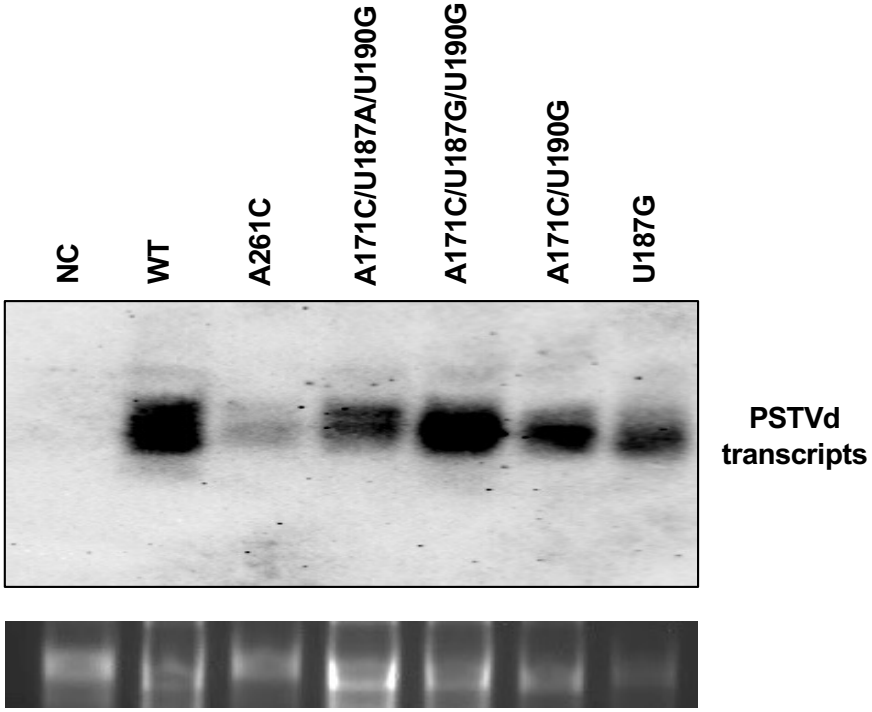
NC
WT
A261C
A171C/U187A/U190G
A171C/U187G/U190G
A171C/U190G
U187G
PSTVd
transcripts

Figure S1

Identical to PSTVd C-loop

potato spindle tuber viroid

citrus exocortis viroid

citrus viroid IV

chrysanthemum stunt viroid

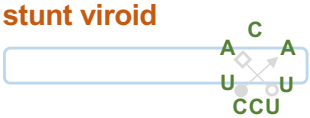

tomato apical stunt viroid

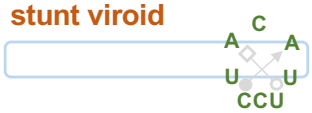

tomato chlorotic dwarf viroid

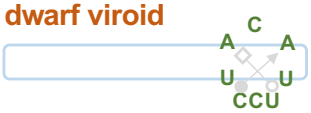

iresine viroid-1

tomato planta macho viroid

pepper chat fruit viroid

Citrus bark cracking viroid

mexican papita viroid

C-loop variants

columnea latent viroid

coconut cadang cadang viroid

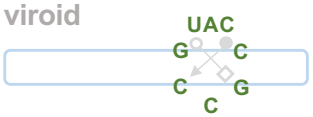

apple scar skin viroid

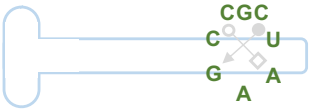

coleus blumei viroid-3

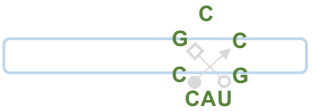

coleus blumei viroid-1

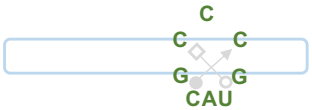

coleus blumei viroid-2

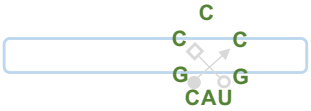

citrus viroid-V

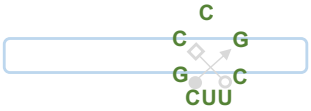

apple dimple fruit viroid

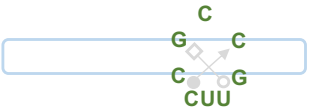

grapevine yellow speckle viroid-2

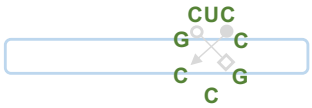

coconut tinangaja viroid

australian grapevine viroid

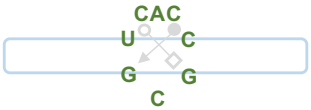

citrus viroid-VI

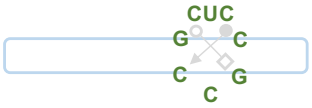

pear blister canker viroid

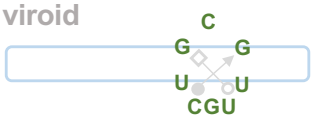

hop latent viroid

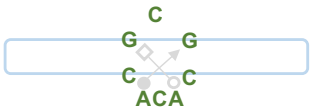

grapevine yellow speckle viroid-1

dahlia latent viroid

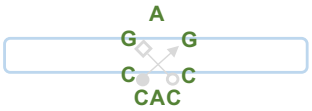

grapevine latent viroid

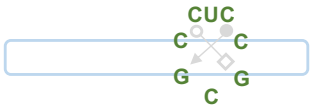

citrus bent leaf viroid

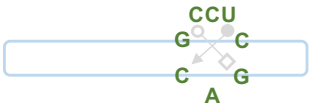

hop stunt viroid

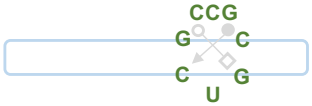

Figure S2

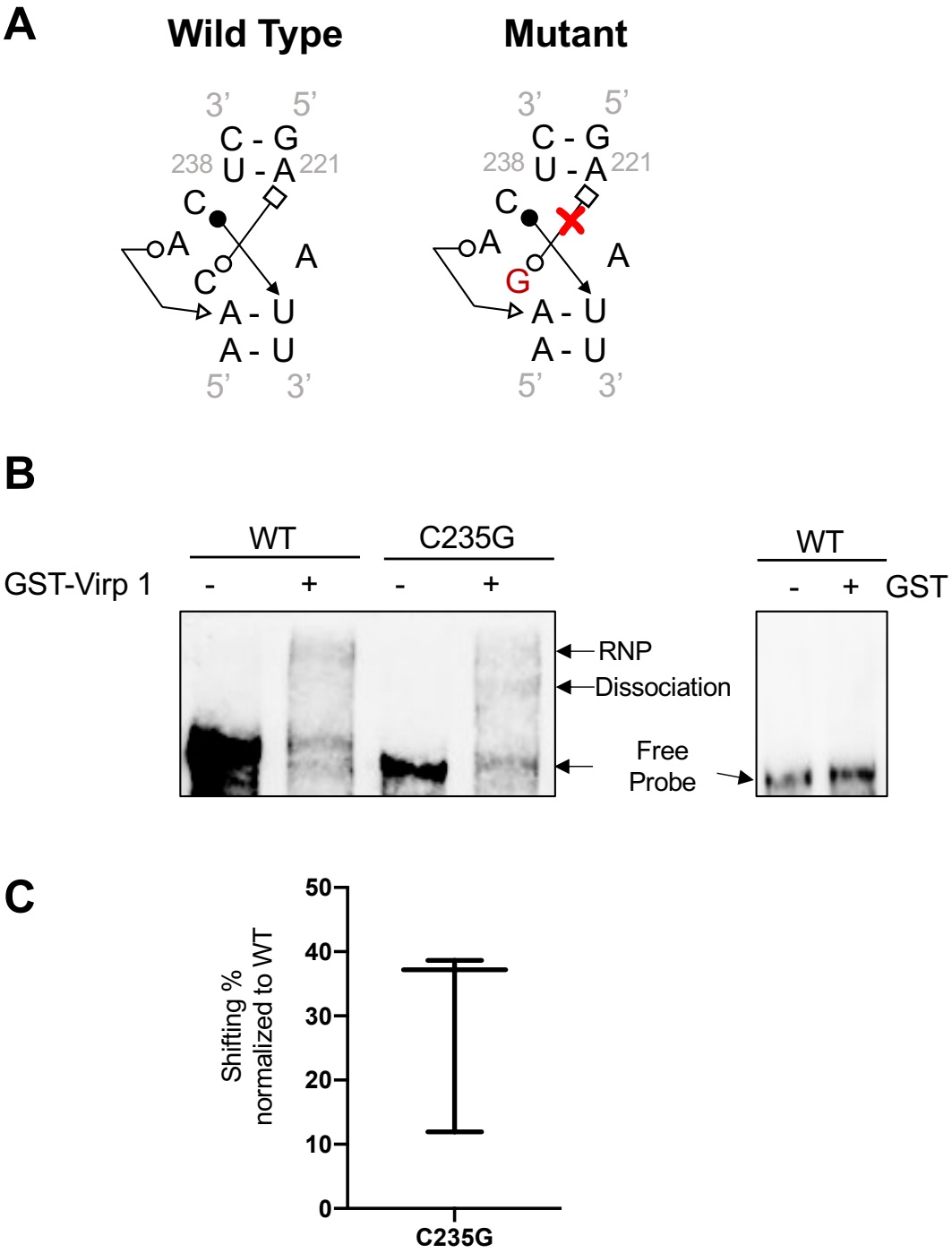
A
Wild Type
Mutant
3'
5'
C - G
238 U - A 221
C
A
A
C
A - U
A - U
5'
3'
G
B
WT
C235G
WT
GST-Virp 1
-
+
-
+
-
+
GST
RNP
Dissociation
Free
Probe
C
Shifting %
normalized to WT
50
40
30
20
10
0
C235G

Figure S3